

Jet Noise Modeling Using Synthetic Anisotropic Turbulence

Mattias Billson ^{*}and Lars-Erik Eriksson [†]and Lars Davidson [†]

Chalmers University of Technology, SE-412 96 Göteborg, Sweden

The hybrid noise prediction technique SNGR (Stochastic Noise Generation and Radiation Method) has been further developed to improve the physics of the synthesized turbulence. The present method includes anisotropy of the synthesized turbulence which is used as source field for the inhomogeneous linearized Euler equations. The anisotropy of the synthesized turbulence includes velocity anisotropy in terms of Reynolds stresses as well as length scale anisotropy in terms of two-point correlations. A new time filtering procedure which determines the time development of the synthesized turbulence is also presented. The present method has been applied to three jet cases. These are (based on jet exit conditions) Mach 0.75 cold ($T_j/T_{amb} = 1$) and hot ($T_j/T_{amb} = 2$) jets as well as a Mach 0.90 cold jet. The ability of the presented method to predict the noise from these jets is evaluated against LES (Large Eddy Simulation) data and measurements. This includes the effect of anisotropy in both near-field and far-field statistics. The degree of anisotropy in the proposed SNGR method is taken from a two-equation $k - \varepsilon$ RANS (Reynolds Averaged Navier Stokes) model together with the Boussinesq assumption. The ability of the two-equation RANS model to predict anisotropy in the near-field turbulence is compared to LES results. The $k - \varepsilon$ RANS model is found to be able to predict most of the anisotropy of the turbulence in the jet shear-layers even though the difference in magnitude in the normal components of the RANS stress tensor are under-predicted. The method to generate anisotropic synthesized turbulence is then validated to the underlying RANS solution and shows good agreement. It is furthermore shown that the agreement of the far-field results between the present SNGR method and the reference data has improved by introducing anisotropy in the synthesized turbulence even though the results are not drastically changed. The far-field sound pressure level directivity computed from the present method is within 3 dB of measurements. Although the spectral content in the far-field sound has improved by the introduction of anisotropy, there are still discrepancies for low frequencies compared to measurements.

Nomenclature

Roman letters

a	normalized Reynolds stress tensor
D	nozzle exit diameter
f	frequency
f_A	amplitude factor

^{*}PhD student, Division of Thermo and Fluid Dynamics, Department of Mechanical Engineering

[†]Professor, Division of Thermo and Fluid Dynamics, Department of Mechanical Engineering

Copyright © 2004 by M. Billson, L.-E. Eriksson and L. Davidson. Published by the American Institute of Aeronautics and Astronautics, Inc. with permission.

f_L	length scale factor
f_τ	time scale factor
h	enthalpy
k	wave number length
\mathbf{k}	wave number vector
\overline{k}	turbulence kinetic energy
L_t	turbulence length scale
M	Mach number
p	pressure
r	radius in cylindrical coordinates
\mathbf{R}	rotation matrix
S_{ij}	Mean strain-rate tensor
St	Strouhal number $St = f D_j / U_j$
T	Temperature
U	mean axial velocity
\mathbf{u}	velocity fluctuation
\hat{u}	mode amplitude
\mathbf{v}	velocity fluctuation
\mathbf{x}	spatial coordinate
\mathbf{xyz}	coordinate system

Greek letters

δ_{ij}	Kronecker delta
Δt	time step
Δx	cell size in x -direction
ε	turbulence dissipation rate
μ	viscosity
μ_T	Eddy viscosity
ψ	phase angle
ρ	density
$\boldsymbol{\sigma}$	direction vector
$\boldsymbol{\tau}$	Reynolds stress tensor
τ_t	turbulence time scale
θ	angle from axial direction

Subscripts

amb	ambient conditions
j	vector index or jet exit conditions
n	mode number

Superscripts

a	anisotropic
$*$	principal axes
\overline{m}	time step number
$\overline{(\cdot)}$	time average
$\overline{(\cdot)}$	Favre time average

I. Introduction

Synthesized turbulence is in the present work used to generate source fields for the inhomogeneous linearized Euler equations with the purpose of performing noise predictions of turbulent jet flows. This is done in the framework of the SNGR (Stochastic Noise Generation and Radiation) method which was first presented by Bechara *et al.*¹ and later further developed by Bailly *et al.*^{2,3} The form of the SNGR method used in the present work differs from the ones above in the way time dependence is introduced in the generation of synthesized turbulence. This modified approach was presented in Billson *et al.*⁴

Common for the SNGR methods above is that locally isotropic synthesized turbulence¹⁻⁵ is used as source field for the inhomogeneous linearized Euler equations. A method to generate anisotropic synthetic turbulence has been developed in Billson *et al.*⁶ and the present paper is focused on evaluating the properties of the newly developed method when applied to high Mach number subsonic jets.

The present method to synthesize anisotropic turbulence requires as input an estimation of the Reynolds stress field, which is given from a two-equation $k - \varepsilon$ RANS solution of the flow. The ability of the $k - \varepsilon$ RANS model to predict anisotropy is compared to results from a Large Eddy Simulation (Andersson *et al.*⁷) of the same flow. Both near-field and far-field statistics of the synthesized turbulence are in turn evaluated and compared to reference data from the LES and measurements by Jordan and Gervais.⁸

The structure of the paper is as follows. First the method to generate isotropic synthetic turbulence is presented. This is followed by a description of how to modify the method to be able to generate anisotropic synthesized velocity fields. Different aspects of anisotropy in terms of velocities, length and time scales are then discussed, including anisotropy of LES, RANS and the synthesized turbulence. Far-field noise predictions from the isotropic and anisotropic SNGR methods are then compared to the measurements. The generality of the method for different jets is assessed by simulating cold and hot jets at Mach 0.75 and 0.90. This is followed by a conclusion of the paper.

II. Methodology

The way synthesized isotropic turbulence is generated in the present approach is fully described in [4,9], and only the most important steps will be presented here. An isotropic synthesized velocity field $\mathbf{u}(\mathbf{x})$ is generated through the sum of Fourier modes^{1,5}

$$\mathbf{u}(\mathbf{x}) = 2 \sum_{n=1}^N \hat{u}_n \cos(\mathbf{k}_n \cdot \mathbf{x} + \psi_n) \boldsymbol{\sigma}_n \quad (1)$$

where \hat{u}_n , ψ_n and $\boldsymbol{\sigma}_n$ are amplitude, phase and direction of the n^{th} Fourier mode. Spatial location is denoted by \mathbf{x} and wave number vector for each mode by \mathbf{k}_n . The direction of each mode in wave space and in physical space is randomized with the condition that $\mathbf{k}_n \cdot \boldsymbol{\sigma}_n \equiv 0$, i.e. the continuity equation for incompressible turbulence is fulfilled. The amplitude \hat{u}_n for each mode is determined by a modified von Kármán-Pao spectrum which is linearly discretized⁴ in wave space (see Billson *et al.*^{4,9} for more details).

Time evolution of the synthesized turbulence is introduced through a time filter which filters statistically independent realizations $\mathbf{u}(\mathbf{x})$ into turbulence with a specified autocorrelation. This is done through the equation

$$\mathbf{v}^m(\mathbf{x}) = a\mathbf{v}^{m-1}(\mathbf{x}) + b(\mathbf{u}^m(\mathbf{x}) + \mathbf{u}^{m-1}(\mathbf{x})) \quad (2)$$

where $a = \exp(-\Delta t/\tau_t)$, $b = f_A \sqrt{(1-a)/2}$ and Δt and τ_t are the time step size and the time scale respectively. Superscript $(\cdot)^m$ denotes time step number and f_A is an amplitude factor to enable control of the kinetic energy of the synthesized turbulence. To account for convection of the generated turbulence field $\mathbf{v}_t^m(\mathbf{x})$ a simple convection equation is solved for $\mathbf{v}^{m-1}(\mathbf{x})$

$$\frac{\partial(\overline{\rho \mathbf{v}^{m-1}})}{\partial t} + \frac{\partial(\overline{\rho u_j \mathbf{v}^{m-1}})}{\partial x_j} = 0 \quad (3)$$

before it is used in equation 2. Two parameters are used to relate the synthesized turbulence to the underlying RANS solution. These are the length scale and the time scale which determine the energy distribution in wave space and the autocorrelation respectively. These are computed from the RANS solution as

$$\begin{aligned} L_t &= f_L \frac{\overline{k}^{3/2}}{\varepsilon} \\ \tau_t &= f_\tau \frac{\overline{k}}{\varepsilon} \end{aligned} \quad (4)$$

where the length and time scale factors f_L and f_τ are used for calibration of the length and time scales.

III. Anisotropy

The method to introduce anisotropy in the generation of synthesized turbulence is fully described in Billson *et al.*⁶ and only the final expressions are presented here. The goal is to introduce anisotropy to the velocity field in the principal axes of a model stress tensor $\boldsymbol{\tau}$ since in these axes, the cross-correlation components in the tensor are all zero and the anisotropy of the flow is determined by the diagonal components of the tensor. Let superscript $(\cdot)^*$ denote variables expressed in the principal coordinate system \mathbf{xyz}^* of the Reynolds stress tensor.

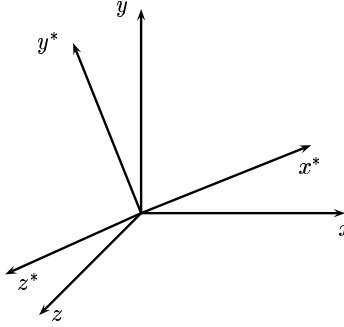


Figure 1. Normal coordinate system xyz and principal coordinate system xyz^* of model Reynolds stress tensor.

A velocity field $\mathbf{u}^{a*}(\mathbf{x}^*)$ which is anisotropic is constructed in the \mathbf{xyz}^* coordinate system (Fig. 1) by the equation

$$\mathbf{u}^{a*}(\mathbf{x}^*) = 2 \sum_{n=1}^N \hat{u}_n \cos(\mathbf{k}_n^{a*} \cdot \mathbf{x}^* + \psi_n) \boldsymbol{\sigma}_n^{a*} \quad (5)$$

where

$$\boldsymbol{\sigma}_n^{a*} = \mathbf{a}^{*1/2} \boldsymbol{\sigma}_n^* \quad (6)$$

The scaling tensor \mathbf{a}^* in Eq. (6) is the normalized Reynolds stress tensor

$$\mathbf{a}^* = -\frac{3\boldsymbol{\tau}^*}{2\rho\overline{k}} \quad (7)$$

expressed in the principal coordinate system associated with the model Reynolds stress tensor $\boldsymbol{\tau}$. The square root denotes the square root of each element. The scaled wave number \mathbf{k}_n^{a*} in Eq. (5) is defined by

$$\mathbf{k}_n^{a*} = \mathbf{a}^{*-1/2}\mathbf{k}_n^* \quad (8)$$

and is introduced to make sure that the resulting velocity field will have zero divergence for a homogeneous anisotropic field, i.e. $\mathbf{k}_n^{a*} \cdot \boldsymbol{\sigma}_n^{a*} = 0$. The final expression for the anisotropic velocity field expressed in the normal coordinate system \mathbf{xyz} is finally computed by

$$\mathbf{u}^a(\mathbf{x}) = \mathbf{R}\mathbf{u}^{a*}(\mathbf{x}^*) \quad (9)$$

where \mathbf{R} is the rotation matrix between coordinate systems \mathbf{xyz} and \mathbf{xyz}^* . The resulting stress tensor associated with velocity field $\mathbf{u}^a(\mathbf{x})$ is the same as that of the model Reynolds stress tensor $\boldsymbol{\tau}$, as shown in Billson *et al.*⁶ Time dependence and convection of the anisotropic turbulent velocity field is done in the same way as for the isotropic case.

IV. Numerical Setup

Three jets simulated using the SNGR method will be presented. These are high Reynolds number jets with jet exit Mach numbers of 0.75 and 0.90 respectively. The Mach 0.75 jet was simulated both as cold and hot where the ratio of the temperature at the jet exit and the ambient fluid were $T_j/T_{amb} = 1$ and $T_j/T_{amb} = 2$ respectively. The flow conditions for the three jets are shown in table 1. The cold Mach 0.75 jet was used to calibrate the parameters in the proposed method and as a test of the generality of the SNGR method the hot Mach 0.75 jet and the Mach 0.90 jet were simulated with the same parameters as for the cold Mach 0.75 jet.

Table 1. Flow parameters for the simulated jet cases. subscripts $(\cdot)_j$ and $(\cdot)_{amb}$ denote jet exit and ambient conditions respectively.

Case	<i>M075c</i>	<i>M075h</i>	<i>M090c</i>	
M_j	0.75	0.75	0.90	
T_j/T_{amb}	1.0	2.0	1.0	
h_{0j}	321841	611137	336162	J/kg
p_{0j}	147116	122685	171329	Pa/m ²
ρ_{amb}	1.2256	1.2256	1.2256	kg/m ³
T_{amb}	288	288	288	K
D_j	0.05	0.05	0.05	m

The numerical code for the linearized Euler equations solves the compressible linearized Euler equations in conservative form on a general structured boundary-fitted, curve-linear non-orthogonal multi-block mesh. In the present state the code uses an explicit four stage Runge-Kutta time marching technique. The convective fluxes are evaluated using a six-point finite volume stencil with dispersion relation preserving coefficients.^{9,10} Upwinding of the convective fluxes based on characteristic variables is used to ensure numerical stability. For more details, see Refs. [9,11]. Kirchhoff¹² integration technique is used to extend the acoustic perturbations to far-field observer points. The Kirchhoff integration surface is placed well in the linear region of the computational domain, but is open at the outflow^{9,13} to avoid hydrodynamic fluctuations on the Kirchhoff surface.

The nozzle geometry is included in the simulation and is the same as the one used in the measurements⁸ and in the LES.⁷ The inflow boundary conditions inside the nozzle are based on specifying the stagnation pressure and enthalpy of the air, see table 1. At the free boundaries, absorbing boundary conditions based on characteristic variables are used. These are modified so that the direction of the one-dimensional analysis^{9,14} is determined by an input parameter⁹ and the direction is chosen so that it points toward the region at the end of the potential core of the jet where most of the sound is generated. A buffer layer^{4,9,15} is applied in the outflow region which attenuates the flow fluctuations before they reach the outflow boundary and there is negligible reflection back into the computational domain.

The same mesh is used for the three jet simulations. It consist of 2 700 000 cells in a combination of Cartesian and polar blocks to be able to have local refinements in the mesh without wasting cells in regions where the resolution requirements are less restrictive. It supports sound waves up to a Strouhal number of $St = 1.5$ with only a small amount of dispersion and dissipation errors.⁹ A more detailed description of the mesh is given in Billson *et al.*⁴

The source region where the synthesized turbulence is generated is the set of cells where $\mu_t/\mu \geq 0.061$. This limit is chosen for numerical reasons and is a bit arbitrary but convenient since the turbulence kinetic energy is very small where this value of μ_t/μ is reached. In the generation of synthesized turbulence $N = 30$ modes were used in each realization of statistically independent velocity fields and the amplitude factor was initially chosen to $f_A = 0.316$. A modified amplitude factor of $f_A = 0.265$ was used when the far-field results were calibrated for the anisotropic model. The statistics from the simulations are taken over 30 000 time steps (when possible) with a time step size of $\Delta t = 8.65 \times 10^{-7}$ [s]. For the cold Mach 0.90 jet and the heated Mach 0.75 jet only 20 000 and 10 000 time steps were used for far-field statistics respectively due to instabilities in the simulations (will be discussed in results). Due to the convective instabilities¹⁶ with low-frequency in the simulations (for all jets), all far-field results are high-pass filtered with a sharp cut-off frequency corresponding to a Strouhal frequency of $St = 0.1$.

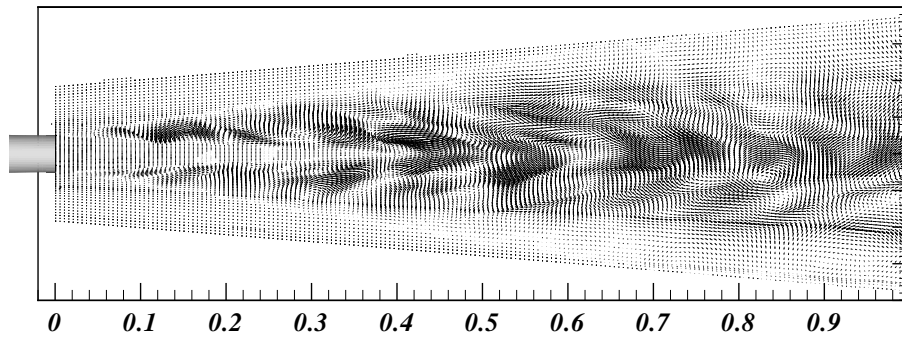
In the anisotropic simulations the normalized Reynolds stress tensor was evaluated from Boussinesq's assumption from the RANS solutions which also constituted the reference solutions for the linearized Euler equations simulations. The eigenvalues and eigenvectors needed for the scaling and transformation of the isotropic turbulence to anisotropic turbulence were computed using LAPAC¹⁷ routines. A realizability¹⁴ condition limiting the turbulence eddy viscosity was applied to the RANS solution before the eigenvalue analysis was performed. Both isotropic and anisotropic simulations were performed and the differences in the results between the different cases will be presented.

V. Near-Field

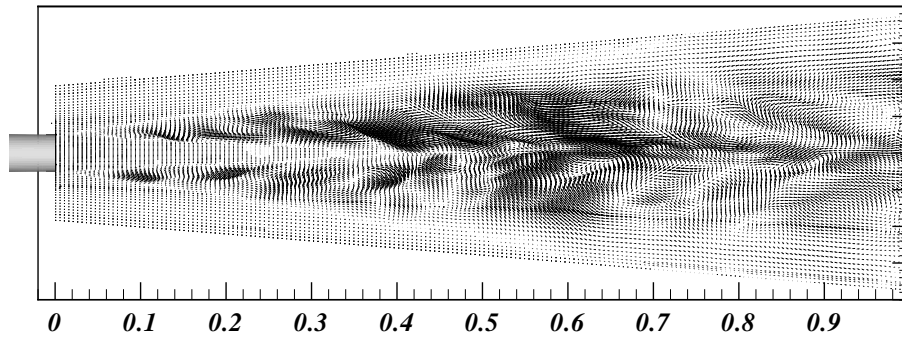
Figure 2 shows vector fields of the synthesized velocities in the xy -plane of the cold Mach 0.75 jet. Figure 2(a) is the isotropic and 2(b) is the anisotropic case respectively. The vector fields show where the source fields are located even if the actual source region extent is larger in the radial and axial directions. The proposed method does not suffer from the spatial de-correlation of the synthesized velocity field in shear flows which has been reported¹⁸ when using similar stochastic methods to generate turbulence. The vector fields in Fig. 2 are taken after 30 000 time steps in the simulation. Both the isotropic and anisotropic vector fields display structure in the synthesized turbulence, but due to truncation of energy in wave-space in the synthesis (highest wave number $k_{max} = 2\pi/(6\Delta x)$),⁴ there are no structures shorter than $\lambda = 6\Delta x$.

VI. Near-Field Statistics

The vector plots of the synthesized turbulence are illustrative, but it is difficult to assess the effect of the anisotropic model on the near-field statistics based on Figs. 2(a) and 2(b). More quantitative information of the synthesized velocity fields are presented below in form of measures of the anisotropy in the shear-layers of the jet. Anisotropy in terms of velocities, length scales and time scales will be discussed.



(a) isotropic



(b) anisotropic

Figure 2. Synthesized velocity vector fields in the xy -plane of a cold Mach 0.75 jet.

A. velocity anisotropy

It is a common conception that two-equation eddy-viscosity RANS models give too little anisotropy since the normal stresses $-\overline{\rho uu}$, $-\overline{\rho vv}$ and $-\overline{\rho ww}$ predicted by Boussinesq (see Eq. (10)) are approximately equal when computed in a typical \mathbf{xyz} coordinate system oriented with one axis close-to aligned with the mean flow.

$$\tau_{ij} = 2\mu_T \left(S_{ij} - \frac{1}{3} \frac{\partial \tilde{u}_k}{\partial x_k} \delta_{ij} \right) - \frac{2}{3} \overline{\rho k} \delta_{ij} \quad (10)$$

This is partly true, and the normal components predicted by Boussinesq are "over-isotropic". This can be seen in Fig. 3 where the normalized normal components of the Reynolds stress tensor at different axial locations in the shear-layer ($r/D_j = 0.5$) of the cold Mach 0.75 jet are plotted for the LES (Fig. 3(b)) and RANS (Fig. 3(a)). The difference between the normal stress components is larger in the LES than in the RANS prediction indicating that the RANS model can not predict the anisotropy of the shear-layer of a jet.

Figure 4 shows the normalized normal stress components from the LES (Fig. 4(b)) and the RANS (Fig. 4(a)) for the same locations as in Fig. 3 but now expressed in the principal axes of each stress tensor. The degree of anisotropy in the LES and RANS can now be more directly compared and the difference is not as

big as indicated in Fig. 3. This is because the cross-correlations ($-\overline{\rho uv}$, $-\overline{\rho uw}$, $-\overline{\rho vw}$) from the RANS are of the same magnitude as those in the LES and these cross-correlations represent much of the anisotropy of the flow in a shear-layer. Thus, in the principal axes of the Reynolds stress tensor, the anisotropy manifested in the cross-correlations is redistributed to the normal components and the degree of anisotropy can be more correctly compared.

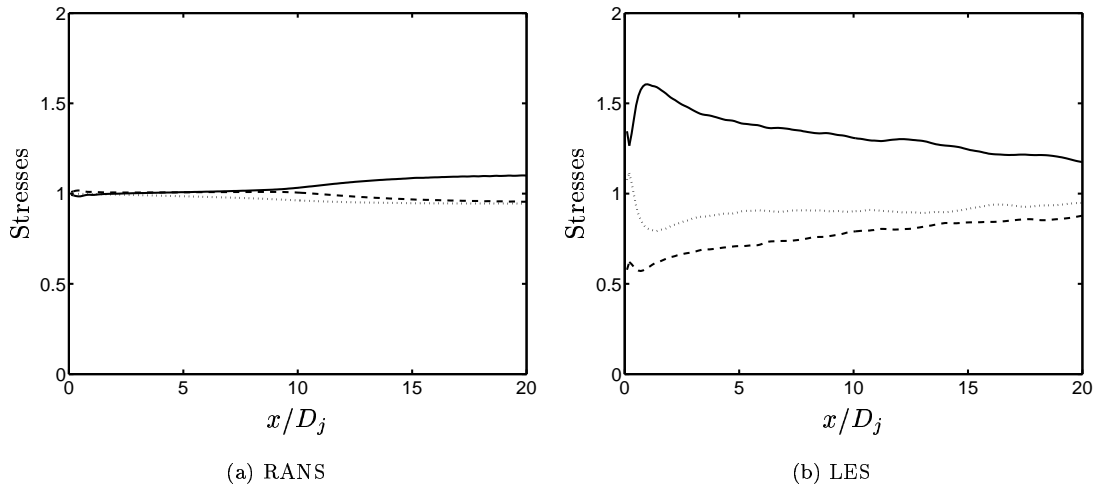


Figure 3. Normal Reynolds stress tensor components in shear-layer. In xy-coordinates. Solid line: a_{11} ; dashed line: a_{22} ; dotted line: a_{33} .

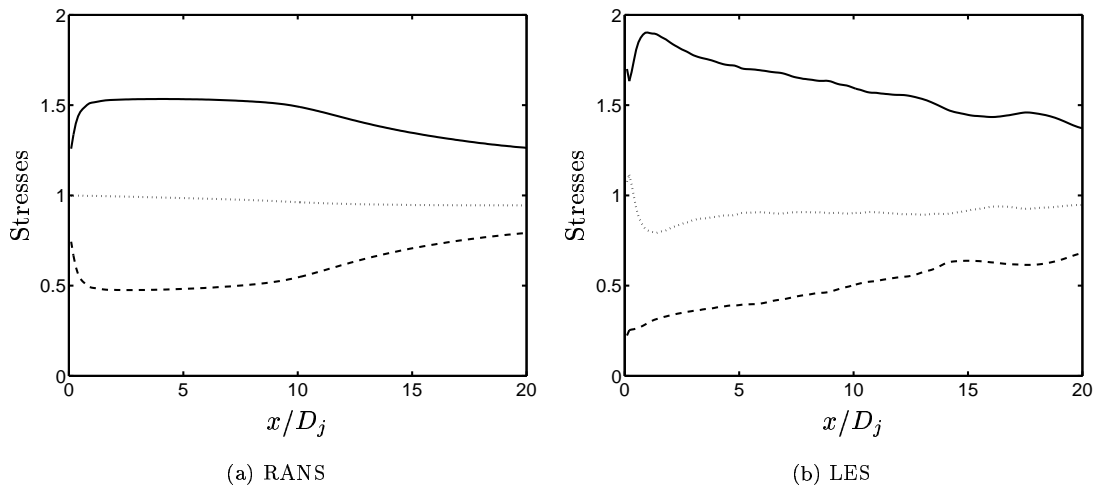


Figure 4. Normal Reynolds stress tensor components in shear-layer. In xy*-coordinates. Solid line: a_{11}^* ; dashed line: a_{22}^* ; dotted line: a_{33}^* .

An other way to illustrate the anisotropy in the shear-layer of a jet is shown in Fig. 5. The data are taken from the LES and the RANS for the cold Mach 0.75 jet at the same axial locations as in Fig. 3. The normal components a_{11}^* and a_{22}^* of the normalized Reynolds stress tensor expressed in the principal coordinate

system \mathbf{xyz}^* are plotted in the angles of the local principal axes. The length of each leg represents the magnitude of each stress and the angle from the x -axis represents the angle of the principal axis compared to the \mathbf{xyz} -coordinate system. As can be seen in the figures the angle is about the same in the LES and in the RANS solutions. The degree of anisotropy (the difference in length of the two legs) is also about the same. The absolute values are not the same but the development of the shear-layers for the two flows show similar behavior. The results show that the $k - \varepsilon$ RANS model can accurately predict the anisotropy of the shear-layer of a high Mach number jet.

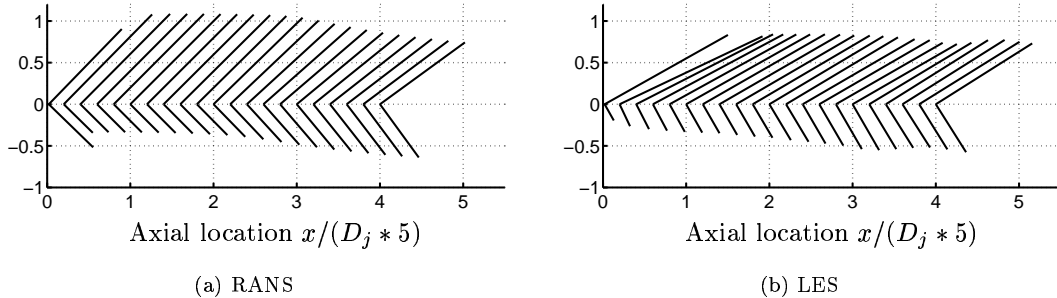


Figure 5. Orientation and magnitude of the normalized normal components of the Reynolds stress tensor expressed in the principal axes. In the shear layer at $r/D_j = 0.5$

A comparison of the RANS anisotropy (manifested mainly in the \overline{uv} -correlation) with the synthesized anisotropic turbulence is shown in Fig. 6. The normalized \overline{uv} -correlation is plotted from the RANS as well as from the proposed method to generate anisotropic velocity fields for the same locations as in Fig. 3. The cross-correlation from the synthesized turbulence is in good agreement with that of the RANS solution.

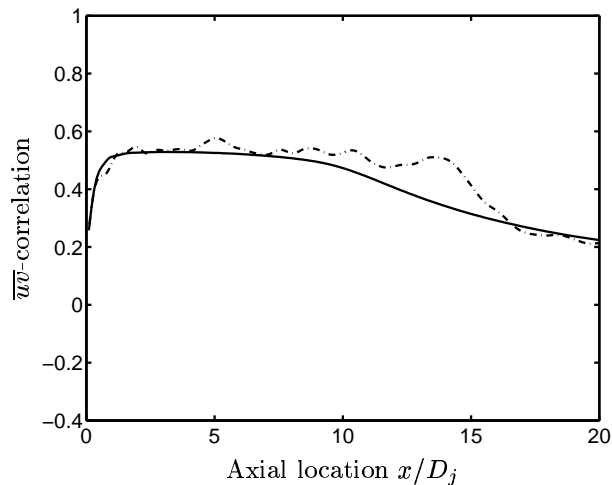


Figure 6. Normalized \overline{uv} -correlation in the xy -plane in the shear-layer at $r/D_j = 0.5$. Solid line: RANS; dash-dotted line: anisotropic SNGR sampling

B. length scale anisotropy

Length scale anisotropy is introduced to the method through the condition of a divergence free velocity field. In the principal axes, the wave number \mathbf{k}_n^a of mode number n is chosen to be perpendicular to the direction

of the mode in physical space σ_n^{a*} . The resulting effect is that the length scales, and correspondingly, the two-point correlations increase in the direction of the increased normal component of the stress tensor. In the same way the correlations decrease in the direction of the decreased component. This is shown in Billson *et al.*,⁶ where the present method to generate anisotropic synthesized velocity fields is assessed using a homogeneous test-case. In a coordinate system where the normal components of the stress tensor are of the same magnitude, the corresponding correlations along the axes are also more equal. Two-point correlations of the isotropic and anisotropic synthesized u -velocity component in the axial and radial directions with the origin at $(x/D_j, r/D_j) = (10, 0.5)$ are shown in Fig. 7. The correlation is increased in the axial direction and decreased in the radial direction for the anisotropic case compared to the isotropic one. This difference is due to the difference in the relative magnitudes of the normal stress components in the region where the correlations are computed (see Fig. 3(a)), which gives a slight modification of the length scales in the x and y directions for the synthesized anisotropic turbulence.

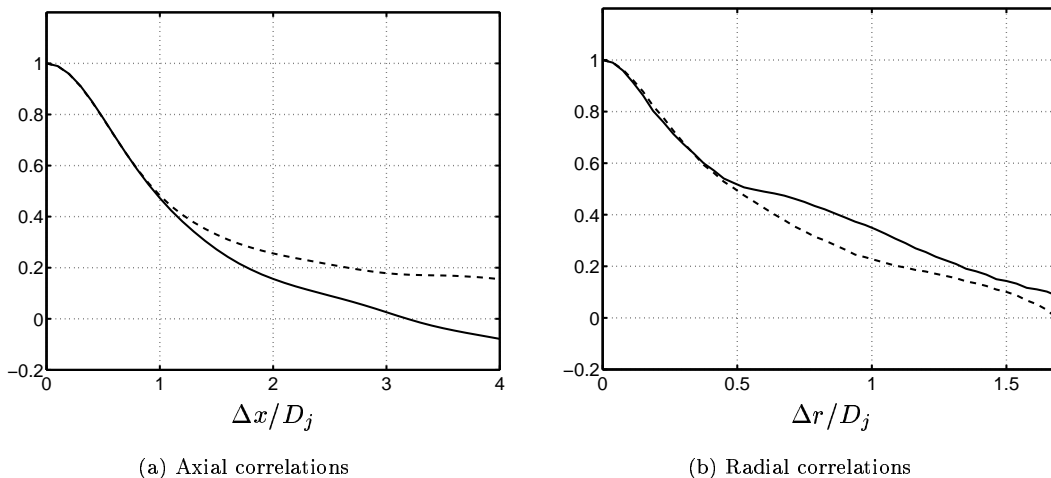


Figure 7. Two-point correlations of the synthesized u velocity component with origin at $(x/D_j, r/D_j) = (10, 0.5)$. Solid line: isotropic, dashed line: anisotropic

C. time scale anisotropy

The present SNGR approach does not have any time scale anisotropy in the sense that the time scales for the different velocity components are equal when measured in the convected reference flow field. The question is if real turbulence in the shear layers of a jet does have such anisotropy or not. This can only be evaluated from two-point space-time correlations in the direction of the mean convection.⁴ Such two-point space-time correlations are available from LES computations by Andersson *et al.*⁷ The correlations are computed in the axial direction at a constant radius and are therefore not strictly in the direction of the mean convection but the difference is small. The convected reference field autocorrelation of the u , v and w velocity components starting from $(x/D_j, r/D_j) = (10, 0.5)$ from the LES are shown in Fig. 8. The results indicate that there could be a time scale anisotropy of the turbulence in the shear-layer of a developing jet, with the correlation of u larger than those of v and w . The degree of anisotropy is though hard to estimate since the correlations do not reach zero.

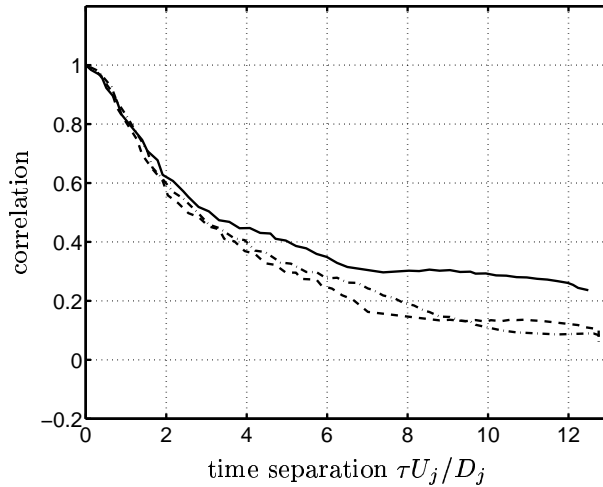


Figure 8. Convected reference field autocorrelations starting from $(x/D_j, r/D_j) = (10, 0.5)$ of u , v and w in convected reference field in shear-layer (LES data). Solid line: u ; dashed line: v ; dash-dotted line: w

VII. Far-Field Statistics

Far-field acoustic results will be presented in terms of over-all sound pressure level (OASPL) directivity and 1/3-octave power spectral density of acoustic pressure. Results from the Mach 0.75 cold and hot jets as well as the Mach 0.90 cold jet will be compared to measurements from Jordan and Gervais.⁸

For the cold Mach 0.75 jet, the OASPL directivity of the emitted sound for the isotropic and anisotropic models are shown in Fig. 9. Also shown are the OASPL directivities from measurements.⁸ The directivity of the isotropic and anisotropic cases are about the same but there is an increase in the emitted sound level in the anisotropic case when the same parameters are used in the two simulations. The anisotropic model does evidently generate more noise compared to the isotropic one. A new calibration of the amplitude factor f_A was necessary in order to correct the emitted noise levels. The results in Fig. 10 were produced from the anisotropic model using $f_A = 0.265$. The directivity and level of the results from the anisotropic case are now in the same agreement with the measurements as those from the isotropic case in Fig. 9(a).

Comparisons of the directivity from the Mach 0.75 hot and cold cases as well as the Mach 0.90 cold case for the anisotropic SNGR model are shown in Fig. 10. The OASPL directivities are generally in good agreement with the measurements except for angles below $\theta = 40$ degrees. The drop below this angle can be attributed to the open Kirchhoff surface in the downstream direction. The trend from the cold Mach 0.75 jet to the cold Mach 0.90 jet in Figs. 10(a) and 10(b) is quite well captured and the agreement with the measurements are relatively good. This is however not the case for the cold to hot Mach 0.75 jets in Fig. 10(a). The reason for this might be twofold. The first reason can be related to that the synthesized source field in the SNGR only contains velocity fluctuations and that sources of sound related to high temperatures are thus not taken into account. The second reason can be related to that the sampling for the hot case is considerably shorter than for the other cases so the statistics is based only on the initial part of the simulation. The reason for this is instabilities which grew rapidly for the hot case. The same type of instabilities also existed in the cold Mach 0.90 jet but the growth rate was much smaller. The sampling of data from these jets were terminated before the instabilities affected the results. The results from the hot Mach 0.75 jet are therefore not as reliable as the results from the cold jets. If the jets are to be simulated for longer times using the present approach, a more stable modified set of equations would be desirable. Such equations could be the acoustic perturbation equations (APE)^{19, 20} which are reported to be stable for arbitrary inhomogeneous mean flows.

The 1/3-octave power spectral density of the far-field pressure at $(r/D_j, \theta) = (30, 90)$ and $(r/D_j, \theta) =$

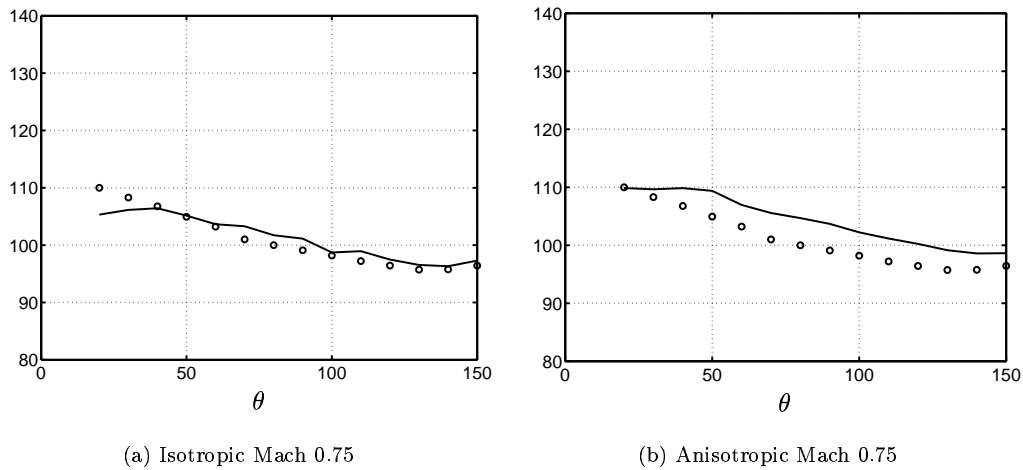


Figure 9. OASPL (dB) at $r/D_j = 30$ for different angles θ from jet axis direction. $f_A = 0.316$ Solid line: present method; circles: measurements

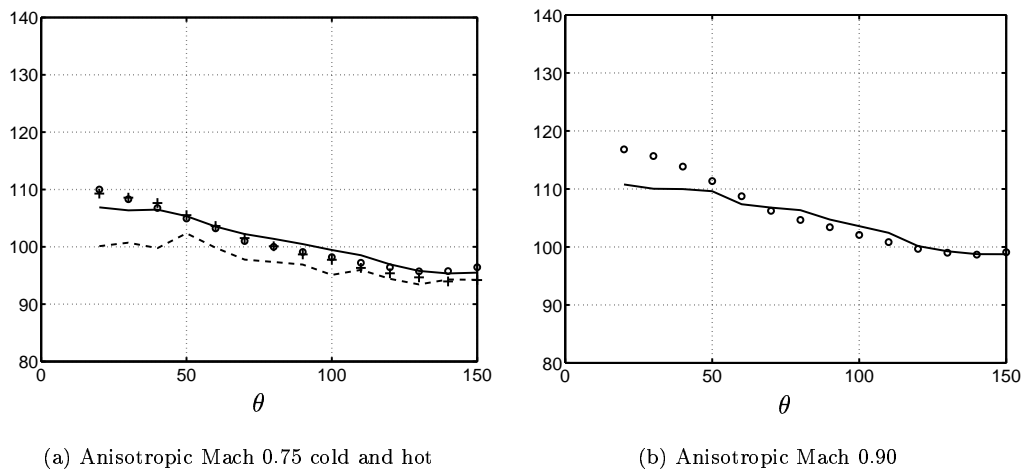


Figure 10. OASPL (dB) at $r/D_j = 30$ for different angles θ from jet axis direction. $f_A = 0.265$ Solid line: present method cold; dashed line: present method hot ; circles: measurements cold; plus signs: measurements hot

(30, 30) are shown for the isotropic cold Mach 0.75 case in Figs. 11(a) and 12(a) respectively. The same spectra for the (re-calibrated) anisotropic case are shown in figs. 11(b) and 12(b). Also shown are the spectra from the measurements.⁸ The overall shape of the spectra for the 90 degree case are in good agreement with the measurements even if there are discrepancies at low frequencies. The difference in the shape of the spectra between the isotropic and anisotropic cases is small. For the 30 degree spectra there is a larger difference between the simulations and the measurements. The peak at low frequencies is not captured in the simulations. The shapes of the spectra are somewhat better for the anisotropic case.

The anisotropy which is evident in the near-field statistics is not as pronounced in the far-field results. A reason for this might be that most of the directivity of a jet is a result of the convective amplification²¹

in the sound generation and the refraction of the generated sound. The convective amplification increases the sound emission in the flow direction and reduces the emission in the up-stream direction. The refraction has the effect (mainly for high frequencies) of directing the sound emitted down-stream out from the axial direction toward the radial direction. These effects are the same for the anisotropic and isotropic simulations and unless the directivity in the sound emission due to anisotropy is strong enough, the resulting sound field directivity is masked by the convective amplification and the refraction.

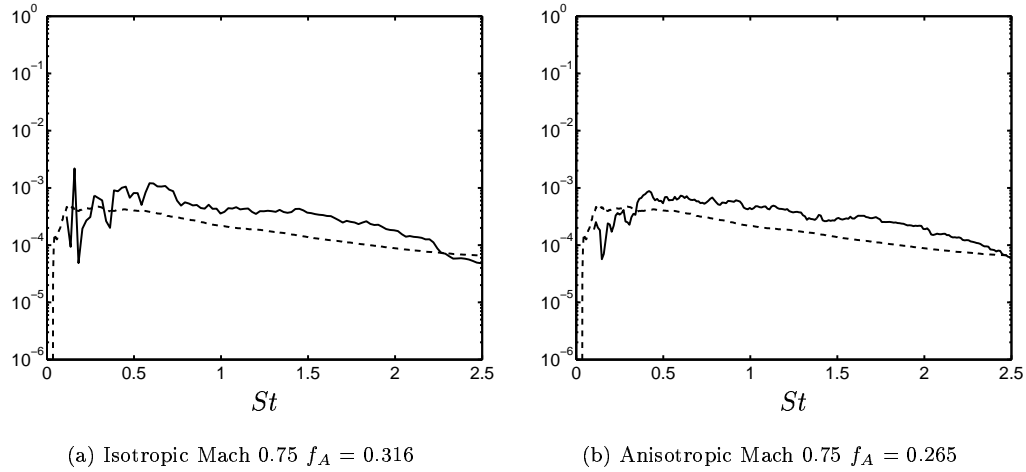


Figure 11. 1/3-octave power spectral density of pressure in an observation point at $(r/D_j, \theta) = (30, 90)$. Solid line: present method; dashed line: measurements

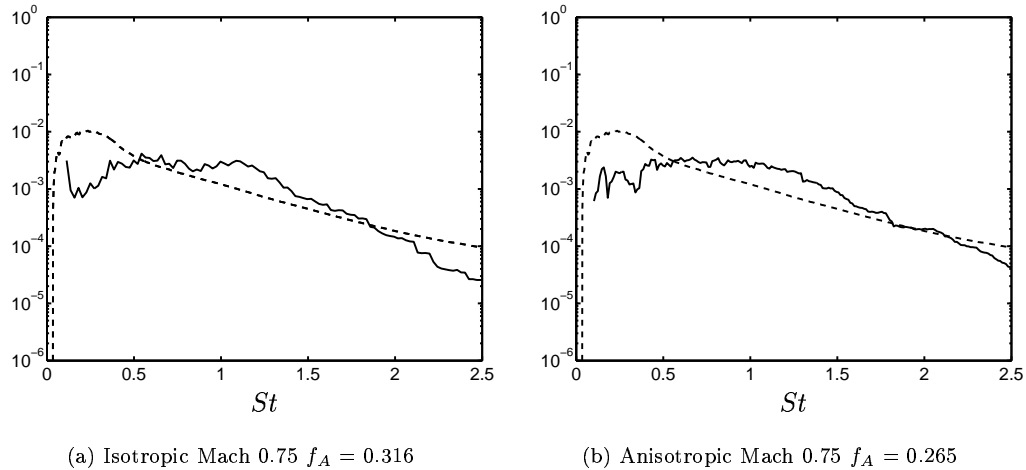


Figure 12. 1/3-octave power spectral density of pressure in an observation point at $(r/D_j, \theta) = (30, 30)$. Solid line: present method; dashed line: measurements

VIII. Conclusion

Noise predictions of three high Mach number subsonic jets have been performed using the hybrid noise prediction method SNGR. The SNGR method has been modified with the inclusion of anisotropy in the generation of synthesized turbulence and the agreement with reference data of the near- and far-field statistics are compared to a model without anisotropy.

The Reynolds stress anisotropy in the synthesized turbulence is based on the solution from a two-equation $k - \varepsilon$ RANS solution of the jet in combination with Boussinesq's assumption. The two-equation $k - \varepsilon$ RANS model is shown to accurately predict Reynolds stress anisotropy when compared to an LES simulation of the same jet flow. Even in the inhomogeneous shear layers of the jet, the proposed method to synthesize anisotropic turbulence is shown to be able to generate turbulence with the same anisotropy as the RANS solution. Length scale anisotropy is included into the stochastic modeling whereas no time scale anisotropy is included.

The sound emission directivity and spectral content in the far-field pressure is compared to measurements. The overall results from the anisotropic model were in better agreement with reference data compared to the isotropic model, but the far-field acoustic results were not greatly altered by the inclusion of anisotropy. The far-field directivity is believed to be dominated by convective amplification in the generation of sound and refraction of the generated sound.

The trend in the emitted sound from a cold Mach 0.75 jet to a cold Mach 0.90 jet is well captured by the model, but not so when a Mach 0.75 jet is heated compared to the unheated jet. The heated jet was found to be more unstable than the unheated jets and the simulation of the hot Mach 0.75 was therefore considerably shorter than for the cold jets.

Acknowledgments

This work was conducted as part of NFFP (National Flight Research Program) as well as the EU 5th Framework Project JEAN (Jet Exhaust Aerodynamics & Noise), contract number G4RD-CT2000-000313.

References

- ¹Bechara, W., Bailly, C., Lafon, P., and Candel, S. M., "Stochastic Approach to Noise Modeling for Free Turbulent Flows," *AIAA Journal*, Vol. 32, No. 3, 1994, pp. 455-463.
- ²Bailly, C., Lafon, P., and Candel, S. M., "A Stochastic Approach to Compute Noise Generation and Radiation of Free Turbulent Flows," AIAA Paper 95-092, 1995.
- ³Bailly, C. and Juvé, D., "A Stochastic Approach To Compute Subsonic Noise Using Linearized Euler's Equations," AIAA Paper 99-1872, 1999.
- ⁴Billson, M., Eriksson, L.-E., and Davidson, L., "Jet Noise Prediction Using Stochastic Turbulence Modeling," The 9th AIAA/CEAS Aeroacoustics Conference, AIAA 2003-3282, Hilton Head, South Carolina, 2003.
- ⁵Kraichnan, R., "Noise Transmission From Boundary Layer Pressure Fluctuations," *J. Acoust. Soc. Am.*, Vol. 29, 1957, pp. 65-80.
- ⁶Billson, M., Eriksson, L.-E., Davidson, L., and Jordan, P., "Modeling of Synthetic Anisotropic Turbulence and Its Sound Emission," The 10th AIAA/CEAS Aeroacoustics Conference, AIAA 2004-2857, Manchester, United Kingdom, 2004.
- ⁷Andersson, N., Eriksson, L.-E., and Davidson, L., "Large-Eddy Simulation of a Mach 0.75 Jet," The 9th AIAA/CEAS Aeroacoustics Conference, AIAA 2003-3312, Hilton Head, South Carolina, 2003.
- ⁸P. Jordan and Y. Gervais, "Modelling self and shear noise mechanisms in anisotropic turbulence," The 9th AIAA/CEAS Aeroacoustic Conference, AIAA 2003-8743, Hilton Head, South Carolina, 2003.
- ⁹Billson, M., "Computational Techniques for Jet Noise Predictions," *Lic. Thesis, Department of Thermo and Fluid Dynamics, Chalmers University of Technology, Gothenburg*, 2002.
- ¹⁰Tam, C. and Webb, J., "Dispersion-Relation-Preserving Finite Difference Schemes for Computational Acoustics," *J. Comp. Physics*, Vol. 107, 1993, pp. 262-281.
- ¹¹Eriksson, L.-E., "Development and validation of highly modular flow solver versions in G2DFLOW and G3DFLOW," Internal report 9970-1162, Volvo Aero Corporation, Sweden, 1995.
- ¹²Pierce, A., *Acoustics. An Introduction to Its Physical Principles and Applications*, Acoustical Society of America, Woodbury, New York, 1991.

- ¹³Freund, J. B., Lele, S. K., and Moin, P., "Calculation of the Radiated Sound Field Using An Open Kirchhoff Surface," *AIAA Journal*, Vol. 34 No. 5, 1996, pp. 909 – 916.
- ¹⁴Eriksson, L.-E., Personal communication, Chalmers University of Technology, Sweden.
- ¹⁵Colonus, T., Lele, S., and Moin, P., "Sound generation in a mixing layer," *Journal of Fluid Mechanics*, Vol. 330, 1997, pp. 375 – 409.
- ¹⁶Huerre, P. and Monkewitz, P. A., "Local and Global Instabilities in Spatially Developing Flows," *Annu. Rev. Fluid Mech.*, Vol. 22, 1990, pp. 473–537.
- ¹⁷"LAPAC, Linear Algebra PACKage, ver 3," 1999.
- ¹⁸Batten, P., Goldberg, U., and Chakravarthy, S., "Reconstructed Sub-Grid Methods for Acoustics Predictions at all Reynolds Numbers," The 8th AIAA/CEAS Aeroacoustics Conference, AIAA 2002-2511, Breckenridge, Colorado, 2002.
- ¹⁹Ewert, R., Meinke, M., and Schröder, W., "Comparison of source term formulations for a hybrid cfd/caa method," The 7th AIAA/CEAS Aeroacoustics Conference, AIAA 2001-2200, Maastricht, The Netherlands, 2001.
- ²⁰Ewert, R. and Schröder, W., "Acoustic perturbation equations based on flow decomposition via source filtering," *J. Comp. Physics*, Vol. 188, 2003, pp. 365–398.
- ²¹Lighthill, M., "On sound generated aerodynamically, I. General theory," *Proc. Roy. Soc.*, Vol. A 211, 1952, pp. 564–587.